

Evaluation of the BET Theory for the Characterization of Meso and Microporous MOFs

Filip Ambroz, Thomas J. Macdonald,* Vladimir Martis, and Ivan P. Parkin*


Surface area determination with the Brunauer–Emmett–Teller (BET) method is a widely used characterization technique for metal–organic frameworks (MOFs). Since these materials are highly porous, the use of the BET theory can be problematic. Several researchers have evaluated the BET method to gain insights into the usefulness of the obtained results and interestingly, their findings are not always consistent. In this review, the suitability of the BET method is discussed for MOFs that have a diverse range of pore widths below the diameters of N₂ or Ar and above 20 Å. In addition, the surface area of MOFs that are obtained by implementing different approaches, such as grand canonical Monte Carlo simulations, calculations from the crystal structures or based on experimental N₂, Ar, or CO₂ adsorption isotherms, are compared and evaluated. Inconsistencies in the state-of-the-art are also noted. Based on the current literature, an overview is provided of how the BET method can give useful estimations of the surface areas for the majority of MOFs, but there are some crucial and specific exceptions which are highlighted in this review.

1. Introduction

Metal–organic frameworks (MOFs) are one of the most highly porous materials and since their discovery, have been thoroughly investigated as a result of their specific properties that are exceptional among known materials.^[1–3] They combine two disciplines, namely organic and inorganic chemistry^[4] and possess many favorable characteristics, for example high surface area, high porosity, tenability, reproducibility, high sorption capacities, facile syntheses, and good possibilities for scale up.^[5–8] Therefore, such materials can be used in numerous applications, for instance catalysis,^[9–11] gas storage,^[12–14] gas separation,^[15–17] drug delivery,^[18–20] luminescence,^[21–23] solar cells,^[24–26] and batteries.^[27–29] This class of porous polymeric material is assembled by the connection of a metal ion linked

F. Ambroz, Dr. T. J. Macdonald, Prof. I. P. Parkin
Department of Chemistry
University College London
London WC1E 6BT, UK
E-mail: tom.macdonald@ucl.ac.uk; i.p.parkin@ucl.ac.uk

Dr. V. Martis
Surface Measurement Systems Ltd.
Unit 5 Wharfside Rosemont Road, Middlesex, HA0 4PE, UK

 The ORCID identification number(s) for the author(s) of this article can be found under <https://doi.org/10.1002/smt.201800173>.

© 2018 The Authors. Published by Wiley-VCH Verlag GmbH & Co. KGaA Weinheim. This is an open access article under the terms of the Creative Commons Attribution License, which permits use, distribution and reproduction in any medium, provided the original work is properly cited.

DOI: 10.1002/smt.201800173

together by organic bridging ligands to form 1D, 2D, or 3D structures as illustrated in **Figure 1**.^[30] Since there are a variety of different metal ions and organic linkers, essentially an infinite number of possible combinations exist.^[31]

Furthermore, since MOFs are also relatively simple to prepare, building components can be well designed which can result in the production of targeted products.^[33–35] Computational calculations have proven to be useful in predictions of interactions between guest hosts and the framework leading to possible synthesis routes for MOFs with required properties.^[36,37] They are often compared to zeolites;^[38–40] however certain characteristics are often not present in zeolites including big pore sizes, high sorption capacities, and complex sorption behavior.^[6,41] New MOF structures with

diverse properties are still emerging with ever increasing specific surface areas, that have to be determined in the course of MOF characterization.^[42–44] In this regard, correct measurements of the surface areas are valuable as this is a very important characteristic of microporous materials. Usually the surface areas of MOFs are predicted by implementing the theory of Brunauer–Emmett–Teller (BET) where the surface areas are derived from gas adsorption isotherms at the boiling point of a gas.^[45,46] Typically, N₂ gas is used for this purpose.^[47,48] However, other gases, for instance Ar or CO₂ or even organic vapors (dynamic vapor sorption) may also be used.^[49–52] While there have been attempts to use H₂, they remained in the form of discussion.^[53] Surface area can also be reported as the Langmuir surface area that is defined in terms of the monolayer being the limit of adsorption.^[54,55] Many researchers have investigated the suitability of the BET theory since it is based on several assumptions that may not be ideal for determining the surface area of microporous materials such as MOFs.^[56–58] Many concerns were focused on the pore-filling mechanism and uneven monolayer formation which is discussed in the sections below. For amorphous porous materials, the most convenient way to determine the surface area is from adsorption isotherms as opposed to crystalline materials where as a result of a known crystal structure, geometric methods can regularly be applied.^[59,60]

In this review, the applicability of the BET method for determining surface areas of MOFs with various pore widths is discussed. Reported drawbacks and limitations of the BET theory which can lead to unreliable results are also covered. For evaluation of the BET method, experimental data have to be

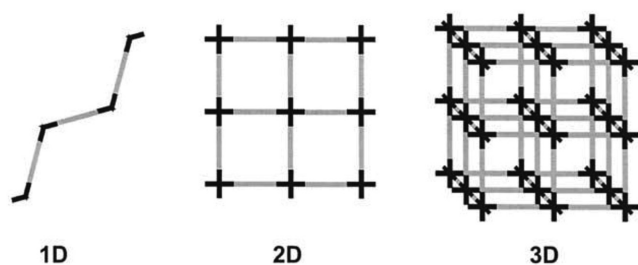


Figure 1. Assembly of 1D, 2D, and 3D network structures of MOFs. Reproduced with permission.^[32] Copyright 2003, Elsevier.

compared. Hence, the surface areas of MOFs obtained with different approaches, namely the values calculated from the crystal structures and from the simulated isotherms (applying BET theory), are examined and compared against the experimental results.

2. BET Theory

The fundamental element of BET theory is associated with the adsorption of a gas on the material's surface.^[61–63] This phenomenon is caused by van der Waals forces that are created by a film of the adsorbate, which consists of atoms, ions, or molecules on the surface of a substance that adsorbs these particles. The process of adsorption can be physical or chemical.^[64,65] While physical adsorption is related to van der Waals forces, chemical adsorption is a result of the chemical reaction between the solid and the adsorbate (gas).^[66,67] The amount of the adsorbed gas on the adsorbent material can be correlated with its surface area.^[68] There are several parameters that have influence on this process for instance, temperature, pressure, characteristics of the material, etc.^[69,70] BET theory is closely related to Langmuir theory. The latter assumes that gas molecules form a monolayer adsorption which is an ideal situation.^[71,72] In such formations, all the molecules that are adsorbed are in contact with the surface of the adsorbent's material. This coverage can occur in a closed-packed structure where molecules are tightly next to each other or they can also be spread around the surface. The gas molecules are held on the surface by gas–solid forces. On the other hand, with multilayer adsorption more than one layer of gas molecules are formed, consequently not all of them are in contact with the surface layer of the adsorbent. Therefore, vapor-phase interaction between gas molecules occurs. These vapor phase interaction energies are similar to gas–solid interaction energies leading to the phenomenon of gas adsorption on the top of gas molecules that are already adsorbed on the surface of a solid. As a result of that, a gas condenses to a liquid phase.^[73] Multilayer adsorption is a typical phenomenon when temperature of the adsorbent's surface is lower than the critical temperature of gas molecules. When layers of adsorbate molecules are formed, the pressure is increasing until it reaches a value similar to the bulk vapor pressure when the bulk condensation occurs.^[73] After monolayer and subsequently multilayer adsorption occurs on the pore walls, capillary condensation follows meaning pores become filled with condensed gas. Such vapor–liquid phase transitions take place below the saturation vapor pressure (P_{sat}) of the bulk liquid. This can occur as a result of



Filip Ambroz is currently an Engineering Doctorate (EngD) student in the Department of Chemistry at University College London (UCL). He received his M.S. degree in molecular modeling and materials science from UCL and B.S. degree in chemical engineering from the University of Maribor, Slovenia. Before starting his

EngD, he did research for a year at the University of South Australia under the supervision of Prof. Thomas Nann. His research is closely linked with the industrial company, Surface Measurement Systems Ltd. In addition, his work includes the synthesis and characterization of microporous materials that can be used for renewable energy generation.



Thomas J. Macdonald is currently a Ramsay Memorial Fellow in the Chemistry Department at University College London. He is also a visiting researcher in the Chemistry Department at Imperial College London. Prior to this, he was a Research Associate in the group of Prof. Ivan Parkin working on the synthesis of

gold nanomaterials. He obtained his Ph.D. at the University of South Australia in 2016 working in the research group of Prof. Thomas Nann where he studied the synthesis of inorganic nanomaterials for water splitting and photovoltaics. His research interests are in the synthesis of functional nanomaterials for renewable energy conversion and storage.



Ivan P. Parkin obtained his B.S. and Ph.D. (supervisor Prof. Woollins) degrees from Imperial College London and did his postdoctoral research at Indiana University with Prof. Chisholm FRS. He was appointed to a temporary lectureship at the Open University before moving to UCL in 1993. Having been head of the Chemistry Department for six

and a half years, he has recently been appointed as Dean of the Faculty of Mathematical and Physical Sciences. His group is mainly concerned with the synthesis of new materials and coatings. He works extensively in chemical vapor deposition, nanoparticle synthesis, antimicrobial coatings, gas sensing, and superhydrophobic surfaces.

the pore's confined space where van der Waals interactions between gas molecules are increased.^[62,74] In BET theory, a multilayer adsorption is assumed where all layers are in equilibrium (and do not interact with each other), therefore the Langmuir equation can be used for each layer.^[75,76] Molecules in the layers below the initial one act as sites for absorption of molecules in the layers above. The bet equation is defined as follows^[74]

$$\frac{P/P_0}{n(1-P/P_0)} = \frac{1}{n_m C} + \frac{C-1}{n_m C} (P/P_0) \quad (1)$$

where n is the specific amount of the adsorbed gas at the relative pressure P/P_0 , n_m is the monolayer capacity of the adsorbed gas, P is the pressure, P_0 is the saturation pressure of a substance being adsorbed at the adsorption temperature, and C is the BET constant which is exponentially related to the energy of monolayer adsorption. From the parameter C , the shape of an isotherm in the BET range can be obtained.

It should be noted that the BET method involves the transformation of a BET isotherm, and from this, a BET plot is obtained.^[77] **Figure 2** shows six different types of BET isotherms.^[78,79]

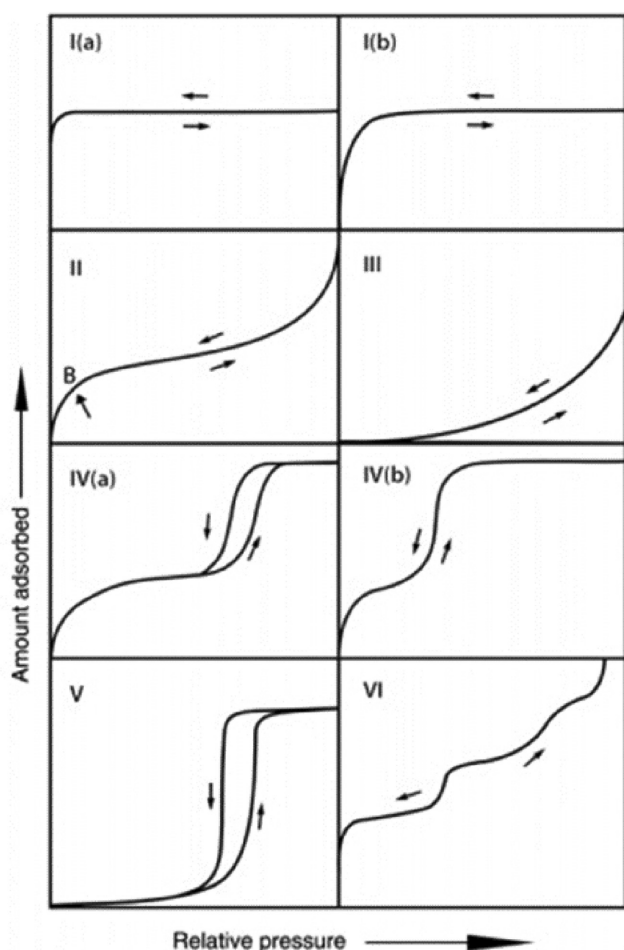


Figure 2. International Union of Pure and Applied Chemistry (IUPAC) classification of BET isotherms. Reprinted with permission.^[74] Copyright 2015, IUPAC.

BET isotherms can be characterized as follows:^[66,74]

- i) Reversible type I isotherm which is typical for microporous solids has two patterns. Type I(a) is obtained for materials having the width of micropores below ≈ 1 nm while type I(b) is for solids that contain both, wider micropores and narrow mesopores ($< \approx 2.5$ nm).
- ii) Reversible type II isotherm corresponds to materials that are nonporous or macroporous. Point B on the isotherm is related to the monolayer coverage. If the monolayer coverage is completed, the curvature change is sharp as opposed to a more gradual curvature which indicates the beginning of the multilayer adsorption (monolayer coverage overlaps).
- iii) Type III isotherm is obtained when the interactions between the adsorbent and adsorbate are weak. Therefore, information about monolayer coverage/formation cannot be provided.
- iv) Type IV isotherm has two patterns which are both related to the width of pores. If the size of width is higher than the critical width, which is related to the material's adsorption characteristics and temperature, a type IV(a) is obtained. Contradictorily, a type IV(b) isotherm is observed for materials having mesopores of smaller widths and is common for mesoporous materials.
- v) The shape of a type V isotherm is seen at over low P/P_0 ranges similar to the shape of a type III isotherm. This phenomenon can be attributed to the weak adsorbent-adsorbate interactions. At higher relative pressure, hysteresis as in the case of a type IV(a) can be observed. Here molecular clustering is followed by the filling of pores.
- vi) Type VI isotherm is typical for multilayer adsorption of materials that have highly uniform nonporous surfaces. The isotherm is in the shape of a stepwise curve, which depends of the material, the gas, and the temperature.

To calculate the BET specific surface area from a BET plot $(P/P_0)/n(1-P/P_0)$ as a function of P/P_0 , a linear BET range on the plot which has to possess high regression coefficient must be selected. Usually, the standard pressure range of 0.05–0.30 is

Table 1. Chemical formulas and different organic linkers of IRMOFs used for the comparison.

IRMOF	Chemical formula ^{a)}	Organic linker
IRMOF-9	$Zn_4O(BPDC)_3$	
IRMOF-11	$Zn_4O(HPDC)_3$	
IRMOF-13	$Zn_4O(PDC)_3$	

^{a)}BPDC = 4,4'-biphenyldicarboxylate; HPDC = 4,5,9,10-tetrahydropyrene-2,7-dicarboxylate; PDC = pyrene-2,7-dicarboxylate.

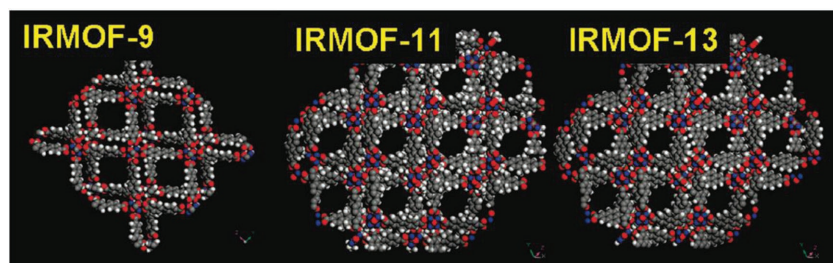


Figure 3. Crystal structures of IRMOF-9, IRMOF-11, and IRMOF-13. Reproduced with permission.^[110] Copyright 2010, American Chemical Society.

used.^[74,80,81] However, since the linearity is not always restricted to this range, Rouquerol et al.^[82,83] recommended four consistency criteria as follows:

- 1) The pressure range selected should monotonically increase with $n(1 - P/P_0)$ as a function of P/P_0 .
- 2) The parameter C resulting from the linear regression should be greater than zero.
- 3) The monolayer loading (i.e., n_m) should correspond to a relative pressure (i.e., P/P_0) within the selected linear range.
- 4) The relative pressure corresponding to the calculated value for the monolayer formation (i.e., $1/(\sqrt{C} + 1)$) should be equal to the pressure determined in criterion 3 (although a tolerance of 20% is acceptable^[80]).

After n_m from the BET equation is obtained, the BET specific surface area (a_s) can be calculated knowing the average area of value σ_m (molecular cross-sectional area) and implementing the following equation^[74,84]

$$a_s = n_m \cdot L \cdot \sigma_m / m \quad (2)$$

where L is the Avogadro constant and m is the mass of adsorbent.

2.1. Drawbacks and Limitations

Despite the extensive use of the BET method, many authors have discussed the limitations that are inherently related when it is applied for the surface area determination of microporous materials. Since the method is based on gas adsorption,

limitations are often related to monolayers. For instance, 1) the validity of n_m (the BET monolayer capacity) is problematic, 2) the monolayer structure is not the same on all surfaces, particularly when N_2 isotherms are used since the molecule is quadrupolar, and 3) at very low pressure ranges (P/P_0) strong adsorption can involve localized monolayer coverage and/or primary micropore filling in the pores of molecular dimensions.^[85] When characterizing materials with micropores below 20 Å, the biggest problem is usually related to micropore filling, which takes

place rather than mono or multilayer coverage. This can lead to obtaining higher or overestimated surface areas; however, high rates of micropore filling can potentially be recognized.^[85–89] Studies also suggest the BET method can be applied for microporous materials without problems of micropore filling if the relevant adsorption data in the correct pressure range are used.^[90] From BET theory, it can also be concluded that appreciable overlap between monolayer and multilayer coverage would impair the assumption that adsorption occurs by multilayer formation.^[56] With materials like MOFs that have very open structures together with high surface area, this assumption is problematic. Several authors also expressed doubts of using the BET method for microporous materials, claiming that is more suitable for the adsorption of adsorbates on the surfaces that are flat.^[86–88,90]

To assess how the reported limitations may reflect the results when using the BET method for different types of MOFs, we compare and evaluate the surface area determination for several approaches.

3. The Agreement between Different Types of BET Surface Areas

The BET method can be used for the characterization of various types of microporous materials including zeolites,^[91–93] photocatalysts,^[94–99] polymers,^[100–102] and photoelectrodes.^[103–108] Since MOFs can contain different sizes of micropores, from “ultramicropores” (below 7 Å) to bigger “super-micropores” (between 7 and 20 Å) or even mesopores (above 20 Å), the

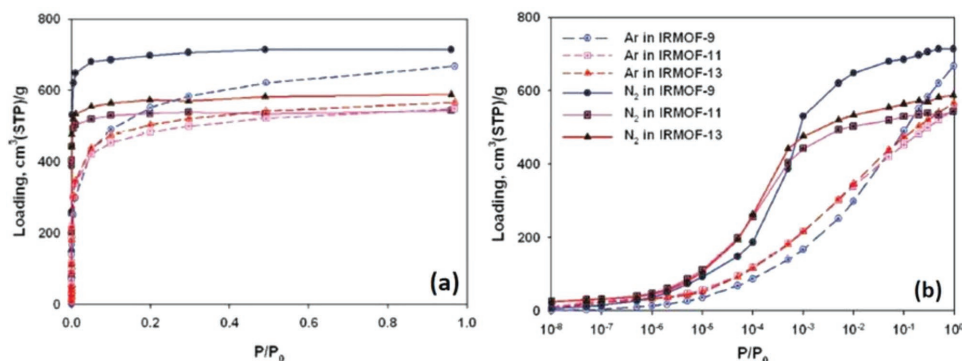


Figure 4. a) Simulated MOF isotherms for N_2 at 77 K and Ar at 87 K on a linear scale. b) Simulated MOF isotherms on a log scale. Reproduced with permission.^[110] Copyright 2010, American Chemical Society.

Table 2. Linear ranges (P/P_0) used for the calculation of the BET surface areas based on the consistency criteria for three different IRMOFs (isoreticular metal–organic framework).

	IRMOF-9	IRMOF-11	IRMOF-13
N ₂ isotherms at 77 K	0.0001–0.0499	0.00005–0.01	0.00005–0.01
Ar isotherms at 87 K	0.0005–0.0499	0.0005–0.01	0.0001–0.01

obtained BET surface areas can potentially be inaccurate. Walton et al.^[56] and Wang et al.^[109] analyzed MOFs with pore sizes larger than 7 Å, while Bae et al.^[110] investigated MOFs containing “ultramicropores.” All authors during the calculation of the BET surface areas followed the consistency criteria as described by Rouquerol et al.^[82] which is particularly important when comparing surface areas of MOF samples that are of the same type so that the quality differences can be addressed. To analyze whether the BET surface areas are meaningful, isoreticular metal organic frameworks (IRMOFs) that have micropore sizes of less than 7 Å and up to 20 Å with the same basic framework topology were selected for comparison.^[110] Table 1 shows that IRMOF-9, IRMOF-11, and IRMOF-13 differ in terms of the

organic linkers. Since these IRMOFs were already investigated by several groups, their experimental characterization can be found in the literature.^[111–113]

The above mentioned IRMOFs were developed by Yaghi and co-workers^[12] and their crystal structure is shown in Figure 3. As illustrated, the crystal structures of IRMOF-11 and IRMOF-13 are similar while the structure of IRMOF-9 consists of a fundamentally different atomic arrangement.

To assess the BET surface areas, grand canonical Monte Carlo (GCMC) simulations were performed and isotherms for N₂ adsorption at 77 K and Ar adsorption at 87 K were calculated for the selected IRMOFs as shown in Figure 4. It can be seen that the obtained isotherms shown in 3a and 3b are type I isotherms.^[114] Since type I isotherms linearly increase at low pressures, gas uptake is strongly enhanced in that region, which was confirmed by simulated snapshots of MOFs where the majority of adsorption sites were occupied at low pressures.^[110] Here, the initial slope corresponds to the size of pores in the material (IRMOF-11 > IRMOF-13 > IRMOF-9) and is the highest for the smallest pore containing material.^[110] It is known, that high surface area is related to high uptake of gas molecules and vice versa.^[115] The amount of adsorbed gas at saturated pressure is the highest for IRMOF-9 and the lowest for IRMOF-11 regardless of the gas isotherm N₂ or Ar, used for the assessment.

Based on the above isotherms, the BET surface areas were calculated for all types of MOFs in the same way that experimental isotherms are usually treated.^[116] Notably, the BET surface areas were obtained from two different pressure ranges, i.e., following the consistency criteria (the linear ranges used are illustrated in Table 2) and using the standard pressure range (P/P_0) between 0.05 and 0.30.^[117] It can be noted from Table 2, that a wider pressure range was always required for N₂ gas. The reason for this phenomenon is that the monolayer is not well defined in Ar isotherms, as discussed in more detail in the work of Gregg et al.^[118] In addition, the pressure range also depends on the type of MOF.

Figure 5 shows the BET surface area comparisons for three IRMOFs (-9, -11, -13) that were obtained by implementing the following methods; the accessible surface areas are based on N₂ and Ar probes from the crystal structures, the BET surface areas from GCMC simulations of N₂ and Ar isotherms that were acquired via computation, while the experimental BET surface areas were acquired via experimental work. The agreement between the accessible surface areas and the simulated ones based on GCMC simulations where the consistency criteria were employed is among the best. This is an interesting finding considering that the BET surface area is calculated from each of the methods in a completely

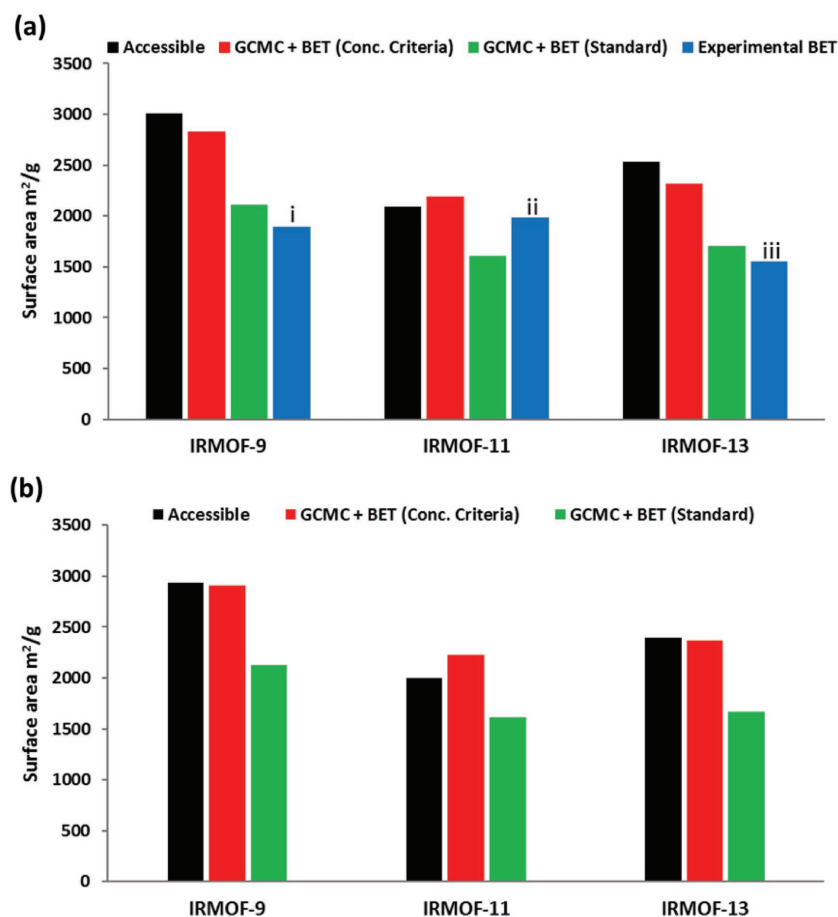


Figure 5. a) Comparison of surface areas obtained based on the calculations from the crystal structures via N₂ probe, BET surface areas from GCMC N₂ isotherms at 77 K (consistency criteria and standard pressure range), BET surface areas from experimental N₂ isotherms at 77 K (i, pressure range not reported; ii, $0.02 < P/P_0 < 0.1$; iii, $0.02 < P/P_0 < 0.3$). b) Comparison of surface areas obtained from the same methods as (a) using Ar probe and GCMC Ar isotherms at 87 K.

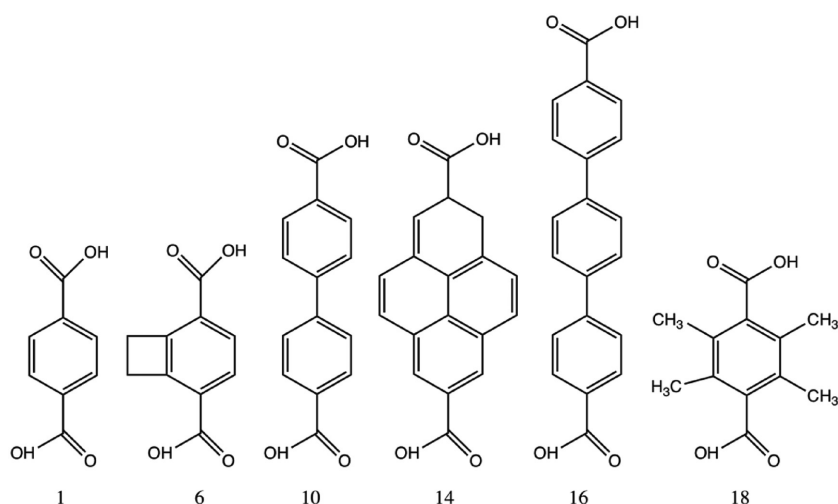


Figure 6. Types of organic linkers attached on IRMOF-1, -6, -10, -14, -16, and -18.

different way. The results suggest that the standard pressure range ($0.05 < P/P_0 < 0.30$)^[119] should not be used for MOFs with pore sizes below 7 Å since the obtained BET surface areas can be incorrect, despite this, a good match can be seen on the graph comparing to experimental values of IRMOF-9 and IRMOF-13.^[110] This can be attributed to the pressure range used for the experimental isotherms which was for IRMOF-13, almost identical ($0.02 < P/P_0 < 0.30$) to the standard pressure range. While the pressure range for IRMOF-9 was not reported, it can be assumed that the calculations were based on the standard pressure range.^[110] It would be of interest to compare the BET surface areas if the consistency criteria could be used since we expect the values would be higher, hence closer to other BET surface areas. It is noteworthy to mention that the pressure range used for IRMOF-11 was lower ($0.02 < P/P_0 < 0.1$). Therefore, a good agreement can be observed for the accessible, GCMC + BET (conc. criteria) and experimental BET surface areas. However, while it is very difficult to achieve a perfect match for experimental results since real samples contain defects or traces of solvent that decrease gas uptake, the results of the study indicate that the BET method can be used for determining surface areas of MOFs containing pores below 7 Å (micropores).

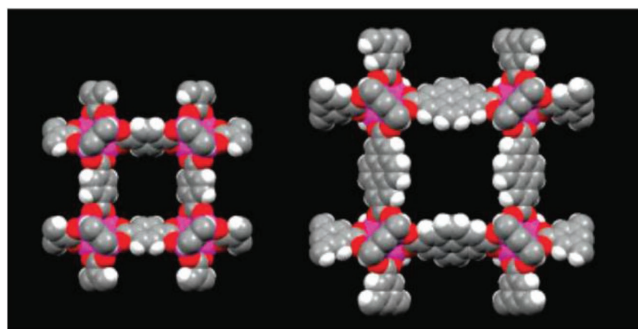


Figure 7. Crystal structures of IRMOF-1 left and IRMOF-14 right containing micropores in the range between 7 and 20 Å. Reproduced with permission.^[56] Copyright 2007, American Chemical Society.

For many years the most widely employed adsorbate for the analysis of surface area and pore structures was N₂. Its adsorption at 77 K has been extensively used for materials that have different sized pores. However, since N₂ molecules exhibit certain characteristics that may not be ideal for such an analysis, Ar molecules have been recently employed as an acceptable alternative, particularly for materials that contain pores below 7 Å. In comparison to Ar molecules, N₂ molecules are known to exhibit a quadrupole moment that can result in unfavorable interactions with surface functional groups and exposed ions.^[120] Such disadvantageous interactions can cause an orienting effect on the adsorbent surfaces together with issues related to the micropore filling pressure.^[120] To circumvent these drawbacks, Ar at 87 K that does not exhibit such

characteristics is commonly implemented. With the absence of a quadrupole moment and higher temperature (87 K), Ar molecules are less sensitive for different arrangements on a material's surface and thus more reliable for pore size analysis and surface area measurements.^[62,80,118] Moreover, the kinetic diameter of less reactive monatomic Ar molecules (3.4 Å) is lower than diatomic N₂ molecules (3.6 Å) which can result in better access to the smallest pores. Therefore, Ar fills small pores such as "ultramicropores" at higher relative pressures which results in faster diffusion and equilibration time.^[120] As reported by Thommes et al.,^[121] with Ar adsorption at 87 K it is also possible to identify differences in pore size in the range of ≈0.1 nm.

However, despite many advantages of using Ar adsorption at 87 K, certain drawbacks still exist and cannot be avoided with the use of N₂ at 77 K. One of them is the restriction of molecules at cryogenic temperatures to enter the pores that are of sized below 4.5 Å. In such situations, CO₂ adsorption at 273 K is usually employed which is discussed in Section 4 of this review. To evaluate surface areas obtained with different techniques also for Ar, a similar comparison was performed for the same MOFs (Figure 5b), where the same trends as in Figure 5a (N₂) were observed. Unfortunately for the study on Ar adsorption performed by Bae et al.^[110] no experimental data were reported. However, considering the conclusions were exact for computationally determined BET surface areas, the authors concluded that it is acceptable to use BET theory for ultramicroporous MOFs where Ar is used as an adsorbate and the pressure range is determined based on the consistency criteria. Nevertheless, for future work it would be interesting to obtain the experimentally determined BET surface areas and compare them with the values in Figure 5b.

To evaluate the applicability of the BET method, a similar study was also performed for IRMOFs (-1, -6, -10, -14, -16, and -18) that consist of only larger micropores (above 7 Å). These IRMOFs have the same basic framework topology but different organic linkers as shown in Figure 6. The organic linkers consist between one and four benzene rings where three different compounds can be attached.

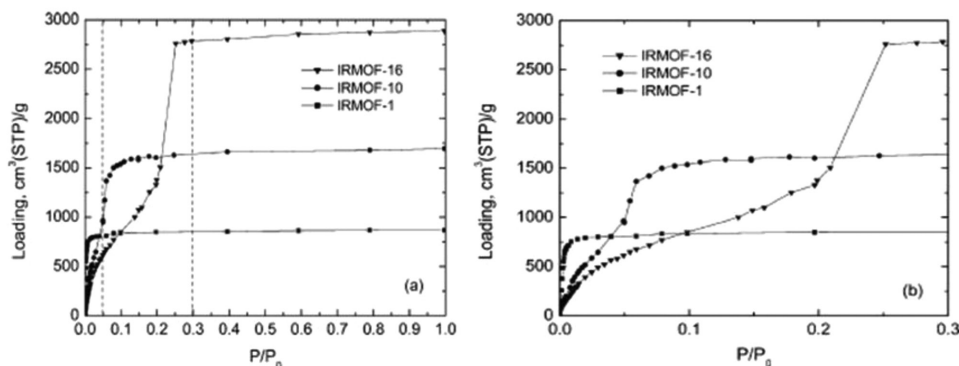


Figure 8. a) Simulated N_2 isotherm at 77 K in IRMOF-1, -10, and -16 with abscissa range between 0 and 1. b) Simulated N_2 isotherm at 77 K in IRMOF-1, -10, and -16 with abscissa range between 0 and 0.3. Reproduced with permission.^[56] Copyright 2007, American Chemical Society.

The crystal structures of IRMOF-1 and IRMOF-14 are shown in **Figure 7**, where the repeating units resemble the shape of a cross. These IRMOFs were developed by Yaghi et al.^[12] for the application of methane storage and were comprise of oxide-centered Zn_4O tetrahedra, linked by molecules of dicarboxylate.^[56]

The adsorption isotherms for IRMOFs with bigger micropores, namely IRMOF-10 and -16 (**Figure 8**), do not have a distinct type I isotherm as opposed to IRMOF-1 that exhibited such a shape. However, the effect of increasing linker size is clearly visible. MOFs with longer organic linkers adsorb more gas which is the result of the more open pore containing structure.^[122] Therefore, the isotherm of IRMOF-16, which has the largest linker size (**Figure 6**), occupied the highest position in **Figure 8a,b**. Contradictorily, IRMOF-1 with only one benzene ring in an organic linker is at the lowest position. One of the biggest differences between isotherms in **Figures 4 and 8** is the step in the latter isotherms. According to the literature,^[12,56] this step was already observed by researchers in the field. Nevertheless, none of them have suggested any clear or relevant explanation.^[56]

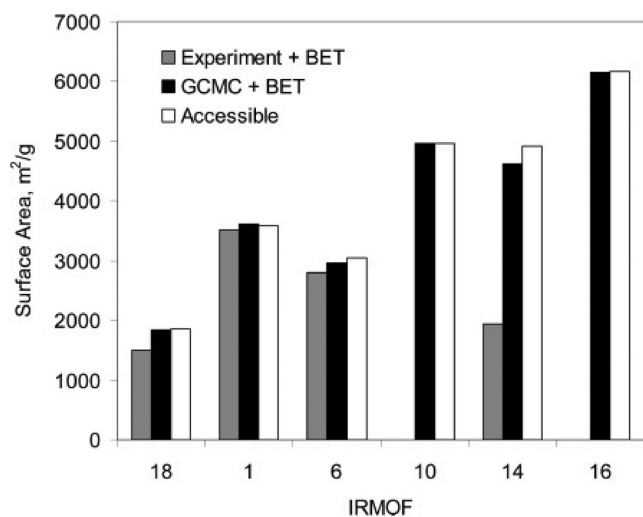


Figure 9. Comparison of surface areas for IRMOFs that consist of larger micropores. Reproduced with permission.^[56] Copyright 2007, American Chemical Society.

Figure 9 illustrates a surface area comparison of IRMOFs using previously discussed approaches. The BET surface areas (black) were calculated from N_2 isotherms (**Figure 8**), gray values are from experimental N_2 isotherms and white surface areas were calculated geometrically from the crystal structures.^[56] The experimental surface area of IRMOF-1 corresponds mostly with the accessible surface area and the surface area measurements obtained from GCMC simulations (consistency criteria). The agreement is also good for IRMOF-6 while the experimental surface area of IRMOF-14 (four benzene rings) does not match well, neither with the accessible nor the GCMC + BET surface area (consistency criteria). Reasons for such a difference could be attributed to a combination of defects in the crystal structure of real samples, interpenetration or insufficient solvent removal during the measurements all of which decreased the N_2 uptake.^[56] The agreement for IRMOF-18 is precise between the surface area calculated from the crystal structure and the simulated one while the experimental value is slightly lower although within reasonable and acceptable limits. Considering IRMOF-10 and IRMOF-16, the experimental BET surface areas were not provided.^[56] Nevertheless, the accessible and the GCMC surface areas are almost identical, a phenomenon that can also be observed for other candidates. It is noteworthy that the reported simulated BET area of IRMOF-10 in the work of Gómez-Gualdrón et al.^[123] is higher ($6736 \text{ m}^2 \text{ g}^{-1}$) than the value in **Figure 8**. However, the difference is most likely a result of the use of a different linear range.

Since the obtained BET surface area is inherently related to the pressure range chosen on the adsorption isotherm, Walton et al.^[56] investigated the adsorption of N_2 molecules at various loadings. It was discovered that N_2 molecules first populate the corner regions followed by the formation of a monolayer until the pores are completely filled. This process occurs below the standard pressure range ($0.05 < P/P_0 < 0.3$) which is commonly used for the calculation of the BET surface area.^[56] Therefore, to obtain accurate data the consistency criteria must be considered to identify a proper pressure range.

Based on a good agreement between the surface areas of MOFs that were obtained by implementing different approaches, the authors^[56] concluded that the BET method can be used for the characterization of MOFs having surface areas in the range of thousands $\text{m}^2 \text{ g}^{-1}$.^[124–126]

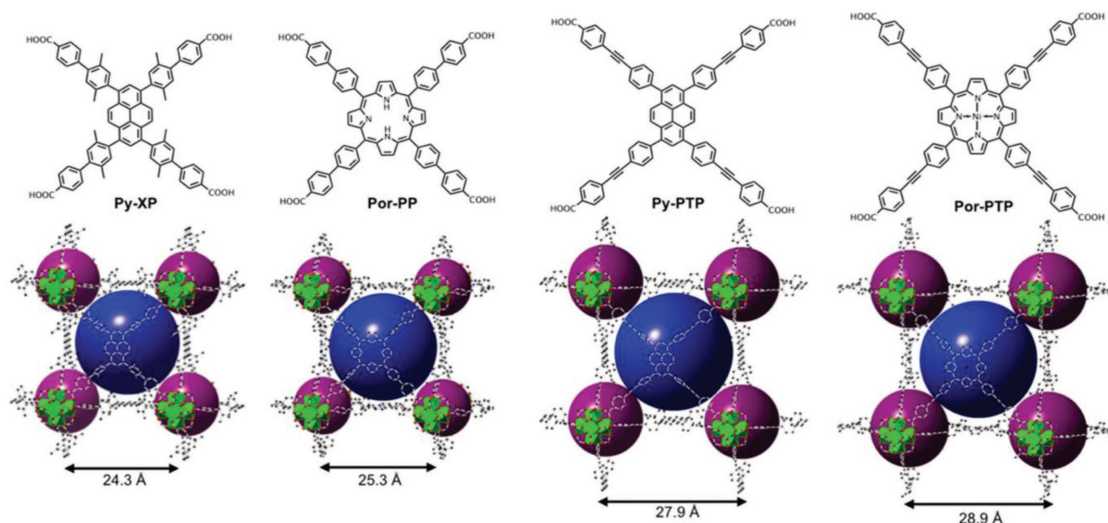


Figure 10. Organic linkers used (Py-XP, Por-PP, Py-PTP, Por-PTP—synthesized and labeled by Wang et al.^[109]) together with crystal structures of NU-1101 to NU-1104 (from left to right) under each corresponding linker. The measured cell parameters are shown on every crystal structure. Reproduced with permission.^[109] Copyright 2015, American Chemical Society (Acronyms described in Table 3).

The surface area agreement of zirconium-based MOFs^[127,128] was analyzed by Wang et al.^[109] where the members of the NU-110x series^[129] that are based on carboxylate linkers were selected (**Figure 10**). Each acronym for this series of MOFs (together with other acronyms mentioned in this review) is described in **Table 3**. These tetratopic organic linkers made of benzene rings form a cross shape and differ in the center arrangement where N₂ can be bound to C-atoms on benzene rings. As illustrated in **Figure 10**, organic linkers influence the size of the unit cell parameters of the cubic cell. This isoreticular series of MOFs exhibit the ftw topology,^[109] which is one example of the 13 known naturally self-dual nets reported to date.^[130]

From the size of pore diameters (**Table 4**) it can be noticed that the NU-110x series of MOFs from NU-1101 to NU-1104 consist of only “super-micropores” (7–20 Å) and mesopores (>20 Å). With increasing linker length (**Figure 10**), the porosity rises together with the size of pores. Therefore, the largest pore diameter is observed for NU-1104, as opposed to NU-1101 where the pore diameter is the smallest.

Since the BET surface area is calculated based on an adsorption isotherm, N₂ isotherms were measured for all four MOFs

at 77 K and are compared with the simulated N₂ isotherms (GCMC simulations) in **Figure 11**. Good agreement between the experimental and simulated isotherms can be seen. This observation is related to the successful activation of the experimental samples meaning solvent molecules and unreacted reactants were totally removed before measurements were performed.

To calculate the BET surface areas, BET theory was applied to N₂ isotherms in **Figure 11**. Since linear pressure range can vary among different MOFs, the consistency criteria^[80] were considered so their surface areas can be compared. **Table 5** shows pressure ranges that were used to calculate the BET surface areas for every MOF. It is notable that for satisfying all the relations of the criteria, a tolerance (around 10%) was needed for both experimental and simulated isotherms.^[109] (Acronyms described in **Table 3**).

While the experimental and the simulated BET surface areas were obtained from N₂ isotherms, the accessible surface areas were calculated from the crystal structures. Here, a rolling-probe method was used meaning a spherical probe in the size of an N₂ molecule was rolled across the crystal structure surface of a particular MOF. As expected from N₂ isotherms in **Figure 11**, the agreement between the simulated and the experimentally determined BET surface areas is excellent for the whole series of MOFs, particularly for NU-1101, NU-1102, and NU-1104. In contrast, the deviation for NU-1103, which has the largest surface area, is slightly higher although within acceptable limits (less than 5%—**Figure 12**). The same trend can also be observed by comparing the accessible surface areas and

Table 3. Description of acronyms used in this paper.

MOF	MOF code	Reference
NU-110x	Northwestern University	[131]
HKUST-1	Honk Kong University of Science and Technology	[132]
MIL-53ht and MIL-47	Materials of Institute Lavoisier	[133]
TIF-1	Tripodal imidazolate framework-1	[134]
UiO-66	University of Oslo	[135]
DUT-32 and DUT-49	Dresden University of Technology	[136]

Table 4. Pore diameters for a series of Zr-based MOFs. (dl = larger pore size, ds = smaller pore size)^[109,137] (Acronyms described in **Table 3**).

	NU-1101	NU-1102	NU-1103	NU-1104
dl [Å]	17.2	20.5	22.7	24.2
ds [Å]	9.5	11.1	12.7	13.5

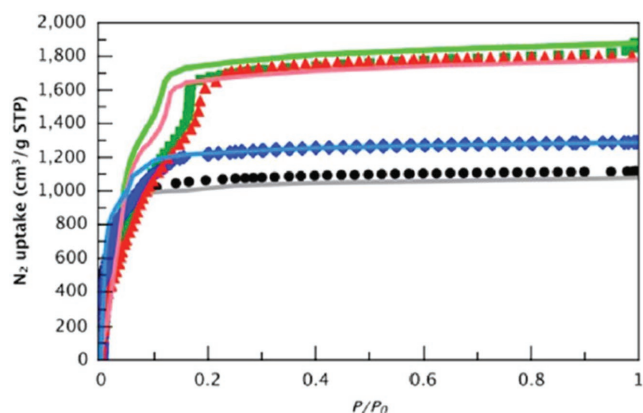


Figure 11. N_2 isotherms for NU-1101 (black), NU-1102 (blue), NU-1103 (green), and NU-1104 (red) where solid lines represent the simulated isotherms while symbols are related to the experimental isotherms. Reproduced with permission.^[109] Copyright 2015, American Chemical Society.

the measurements obtained from N_2 isotherms of NU-1101 and NU-1102. However, the correlation regarding the calculated geometric surface areas of the other two MOFs, namely NU-1103 and NU-1104 is not ideal.

Farha and co-workers^[109] noted a deviation between the experiment and calculation, which is related to the pore filling “contamination.” When the pressure is increased (Figure 13) beyond a structure-dependent value, the curves of simulated N_2 isotherm (blue) and the curves that are related to the formation of a monolayer begin to separate. This can be attributed to pore filling which starts to occur before the monolayer is completed. Hence the monolayer loading is overestimated resulting in excessive surface area.^[109] As can be seen in Figure 13, the amount of adsorbed N_2 not forming the monolayer but being counted toward the monolayer formation is the highest for NU-1103 and NU-1104; the two types of MOFs that show the highest deviation in Figure 12. It is noteworthy that these two candidates consist of pores in the range between microporosity and mesoporosity which could be related to this phenomenon.

As already observed with other studies discussed in this review, the agreement between MOF surface areas that were obtained by different approaches showed the applicability of the BET theory also for many groups of MOFs.

Furthermore, to examine the use of the BET method for materials that are comprised of different pore structures, Düren et al.^[138] studied HKUST-1^[139] and MIL-53ht^[140] (Table 6 and Figure 14). The former material consisted of a 3D channel system with a combination of small and large empty spaces while the pores in MIL-53ht are 1D and in the shape of a diamond. While the width of the pores in both materials does not exceed 20 Å (micropores), MIL-53ht contains only pores below

Table 5. Selected pressure ranges (P/P_0) to calculate the BET surface area for each corresponding sample (Acronyms described in Table 3).

N_2 isotherms at 77 K	NU-1101	NU-1102	NU-1103	NU-1104
Measured	0.054–0.081	0.057–0.147	0.036–0.164	0.045–0.176
Simulated	0.004–0.063	0.004–0.050	0.045–0.089	0.035–0.100

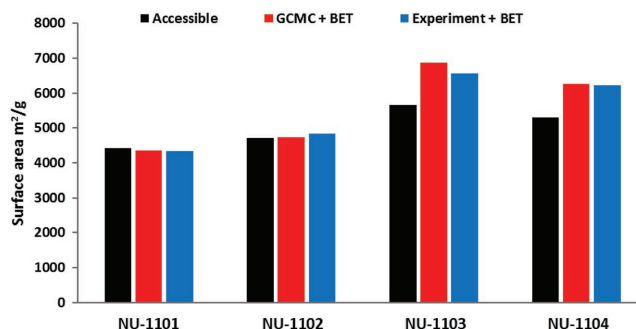


Figure 12. Comparison of surface areas for NU-110x series of MOFs (Acronyms described in Table 3).

7 Å as opposed to HKUST-1 where the range is between 4.7 and 12.1 Å.^[138]

As illustrated in Figure 15, the accessible surface areas and the experimental BET surface areas agree relatively well ($\approx 10\%$ deviation for HKUST-1 and $\approx 11\%$ for MIL-53ht) for both materials. The calculated values from the crystal structures are higher than the experimental ones, which is a result of defects in experimental samples as discussed above. While the BET surface area obtained from simulated N_2 isotherms (GCMC simulations) was not provided for HKUST-1 and MIL-53ht, the authors concluded that the agreement between the accessible and the experimental surface areas was satisfactory.^[138] As a result, they suggested the experimental BET surface areas can be compared against the accessible surface areas to access information about the quality of the synthesized samples. Furthermore, calculating simulated BET surface areas (GCMC simulations) is time consuming and may require additional experimental characterization with techniques such as X-ray diffraction (XRD) and NMR. In contrast, calculating geometric surface areas from the crystal structures is much less time consuming, making it a quick and easy route for the first characterization of MOF samples.^[138]

4. Use of CO_2 Isotherms to Determine the BET Surface Area

When characterizing MOFs that contain small pores close to the kinetic diameters of Ar or N_2 , it may be useful to employ a different approach since these types of molecules cannot pass through the material's pores at cryogenic temperatures (due to inability to overcome the activation energy barriers). Therefore, the BET surface area obtained from N_2 or Ar isotherms can prove unreliable. An alternative way to characterize such materials is by implementing CO_2 , which was reported for porous carbons.^[142] However, reports exist where authors claimed that by employing the latter method, the BET surface area can be inaccurate.^[118]

To examine the applicability of using CO_2 isotherms at 273 K to obtain the BET surface areas of MOFs in a similar way that it was performed for N_2 and Ar isotherms, Kim et al.^[51] selected different types of porous materials and classified them based on their pore sizes into four groups. Group 1 consisted of IRMOF-1 and IRMOF-6; group 2 had IRMOF-9 and IRMOF-11,

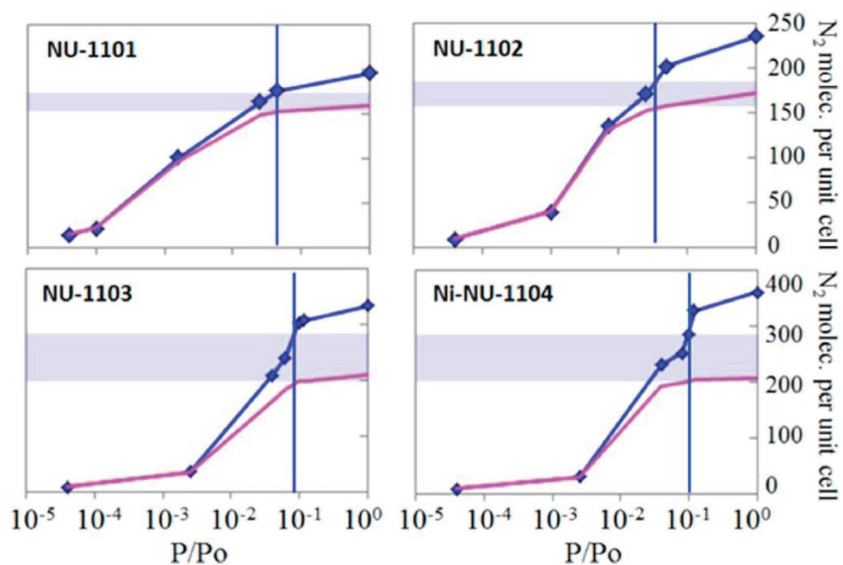


Figure 13. The total number of N₂ molecules (blue) and N₂ molecules in monolayer contact (pink). The vertical line represents the pressure related to the monolayer formation while the shaded area demonstrates the amount of N₂ that is not forming the monolayer but is included in the total surface area. All curves were obtained via simulation. Reproduced with permission.^[109] Copyright 2015, American Chemical Society (Acronyms described in Table 3).

and group 3 had MIL-47 and TIF-1 (micropores in the range between 7 and 9 Å). While the types of organic linkers for materials in group 1 and 2 are illustrated in Figure 6 and Table 1, the organic linkers for MIL-47 and TIF-1 are presented in Table 7. The crystal structures of MOFs in this study are shown in Figures 3 and 7 and Figure 16.

The BET surface areas using the consistency criteria were obtained based on CO₂ isotherms. As opposed to N₂ or Ar isotherms, a linear range to calculate the BET surface areas was very difficult to determine for all groups of materials as a result of unusual BET plots.^[51] Kim et al.^[51] reported that for IRMOF-1, the BET plot at low pressures showed relatively low CO₂ adsorption which causes an overshoot in the initial part of the plot. Consequently, the determined linear range was at relatively high pressures ($0.2 < P/P_0 < 0.25$); this can result in an inaccurate BET surface area determination. A similar behavior was also reported for other MOFs, therefore the selection of a proper linear region was hard to determine for every material. This phenomenon was attributed to relatively weak

Table 6. Organic linkers employed for HKUST-1 and MIL-53ht (Acronyms described in Table 3).

Material	Chemical formula	Organic linker
HKUST-1	Cu ₃ (BTC) ₂	
MIL-53ht(Cr)	Cr(OH)BDC	

CO₂-adsorbent interactions at the temperature of adsorption (273 K).^[51] Table 8 shows linear regions for the BET surface area calculations where the consistency criteria were taken into account.

Comparisons for the six materials studied are illustrated in Figure 17. The highest deviation can be noted for IRMOF-1 (30.3%) that belongs to materials in group 1 where the size of micropores is above 9 Å. Group 1 IRMOFs also corresponds to the highest average deviation, i.e., 24.7% as opposed to group 2 IRMOFs (IRMOF-9 and IRMOF-11) with a broad range of pores between 3.6 and 11.7 Å with an average deviation of 14.3%. Comparing these findings with the surface areas of the same materials that were obtained using N₂ or Ar molecules (Figures 5 and 9) we notice that the deviations between the simulated BET and the accessible surface areas are significantly higher for the values obtained using CO₂ molecules for all series of IRMOFs. Therefore, we believe the employment of CO₂ adsorption isotherms to obtain the BET

surface areas of MOFs should be avoided if possible. Moreover, since Kim et al.^[51] did not provide any experimental BET surface areas of materials examined in their study, they should also be compared with the values in Figure 17 to further evaluate the relation between them in the same way as the N₂ obtained BET surface areas discussed in this review.

5. Geometrically Calculated versus Simulated BET Surface Area

Gómez-Gualdrón et al.^[123] performed a similar study where the accessible and simulated (GCMC) BET surface areas were compared. Their candidate materials were divided based on their topologies, namely pcu, fcu, ftw, and rht. In this review, the evaluation of IRMOFs with pcu topology (IRMOF-1, IRMOF-10, IRMOF-16, etc.) was already discussed (Figure 9). The same applies also for materials with ftw topology (NU-1101, NU-1102,

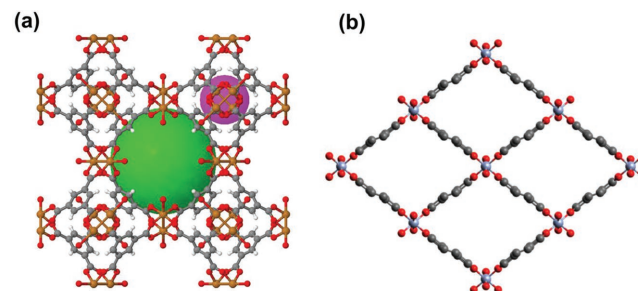


Figure 14. Crystallographic structures of a) HKUST-1 and b) MIL-53ht. Reproduced with permission under the terms of the CC-BY 4.0 license.^[141] Copyright 2017, the Authors. Published by Frontiers Media. (Acronyms described in Table 3).

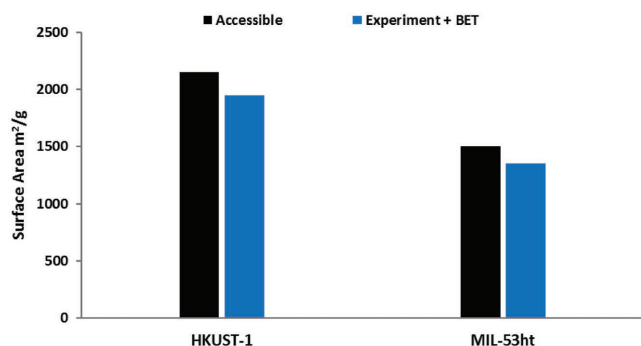


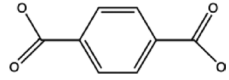
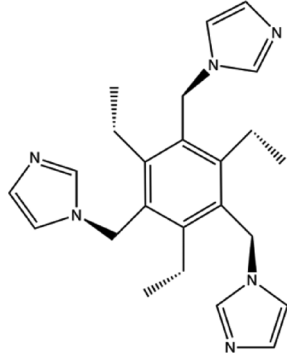
Figure 15. Accessible surface area versus experimental surface area for HKUST-1 (pressure range 0.02–0.1) and MIL-53ht (pressure range 0.0001–0.03) (Acronyms described in Table 3).

NU-1103, and NU-1104) in Figure 12. Candidate materials that feature the other two topologies are UiO-66 for fcu and NU-110 for rht topology, respectively. Schematics of these topologies which determine the pore structures are illustrated in **Figure 18**. It is noteworthy that pcu-PPP mentioned below is of pcu topology. Moreover, the latter material is a hypothetical MOF where “pcu” is related to its topology and “PPP” signifies linkers that constitute of four consecutive phenyl rings.^[123]

To predict the BET surface areas, N₂ isotherms were obtained using GCMC simulations and are shown in **Figure 19**. It should be noted that the pressure ranges used for the BET surface area calculations were determined following the four consistency criteria.^[80] However, as reported by Gómez-Gualdrón et al.^[123] there were cases where it was not possible to fulfill all four points of the criteria. This phenomenon occurred for a material UiO-66 where the fourth point of the criteria could not be satisfied. In these situations, every effort should be made to minimize the error so the BET areas can be compared within different materials or against an idealized crystal structure.

Based on N₂ isotherms from Figure 19, the simulated BET surface areas were obtained and are compared with the accessible surface areas in **Figure 20**. It should be mentioned that in Figure 20 only one material from pcu, fcu, and rht topologies is included while in the Supporting Information of the study of Gómez-Gualdrón et al.^[123] more candidate materials from every topology group are presented. High disagreement (≈33%) can be seen for NU-110 despite fulfilling the four consistency criteria. Interestingly, if another pressure range is used that is not satisfying the consistency criteria, the BET surface areas fall

Table 7. Organic linkers for MIL-47 and TIF-1^[51] (Acronyms described in Table 3).

Material	Pore diameters [Å]	Organic linker
MIL-47	7.5	
TIF-1	7.8	

closer although still with notable overestimation of the simulated value (≈16%).^[123] Such a correlation has not been observed in other studies discussed in this review. Contradictorily, the trend for pcu-PPP is reversed since the accessible surface area is smaller compared to the simulated one. Again, the values do not match despite the lower error than for NU-110. As already mentioned before, it was not possible to cover the four consistency criteria for UiO-66. Thus, the agreement between the two BET surface areas for this material was not acceptable.

An overview in terms of comparison between the accessible surface areas and the simulated ones for MOFs with different topologies and whether the four consistency criteria were fulfilled is illustrated in **Figure 21**. Deviations between the surface areas can be mostly seen in the range between 0–2500 and 5000–8000 m² g⁻¹. In the middle range, the agreement is better and independent whether all points (3rd and 4th) of the consistency criteria were fulfilled or the MOF topology.

As opposed to the study of Düren et al.,^[138] Gómez-Gualdrón et al.^[123] suggested that the experimental BET surface areas should be compared with the simulated BET surface areas that are obtained from simulated N₂ isotherms (GCMC simulations) and not with the accessible surface areas calculated from the crystal structures. Moreover, the above statement was supported together with the results discussed above with their comparison

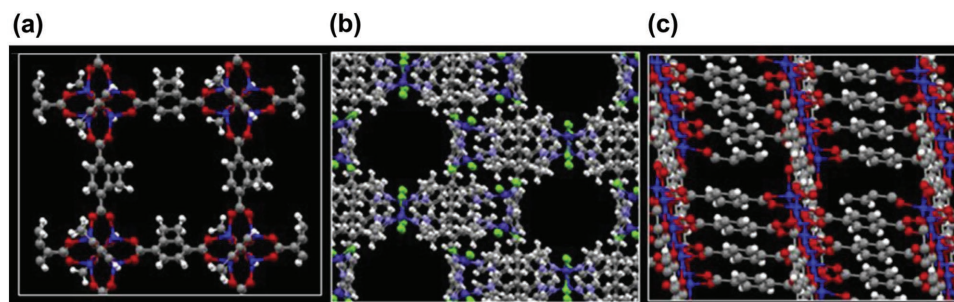


Figure 16. Crystal structures of a) IRMOF-6, b) MIL-47, and c) TIF-1. Reproduced with permission.^[51] Copyright 2016, Elsevier (Acronyms described in Table 3).

Table 8. Determined linear regions (P/P_0) for materials in groups 1–3 (Acronyms described in Table 3).

	IRMOF-1	IRMOF-6	IRMOF-9	IRMOF-11	MIL-47	TIF-1
CO ₂ isotherm at 273 K	0.2–0.25	0.14–0.20	0.10–0.15	0.07–0.15	0.03–0.10	0.06–0.13

of the experimentally synthesized sample of NU-1103 that has a geometrically calculated surface area of 5646 m² g⁻¹. In their previous study which was discussed in this review,^[109] they synthesized an NU-1103 sample and obtained a BET surface area of 6520 m² g⁻¹ which matched well with the simulated one, i.e., 6820 m² g⁻¹. However, if a low-quality sample was obtained, and the experimental BET surface area would be in the range of the accessible, a successful synthesis could be concluded although that would not necessarily be correct.

6. Conclusions

This review has summarized work that has been performed involving the applicability of the BET method for determining surface areas of MOFs. In these studies, the BET surface areas were obtained by implementing three different approaches. While the accessible surface areas were calculated based on the crystal structures of MOFs where the positions of the framework atoms are known from the structure and properties of the crystals, the experimental and the simulated surface areas were obtained from gas (N₂, Ar, CO₂) adsorption isotherms. These adsorption isotherms were either experimentally determined or simulated using GCMC simulations. It is noteworthy, that depending on the pressure range chosen on the adsorption isotherm, the BET surface area may vary widely.^[138] To avoid any uncertainty when determining the BET surface areas and to make comparisons between different materials meaningful, Rouquerol et al.^[82] proposed four consistency criteria that should

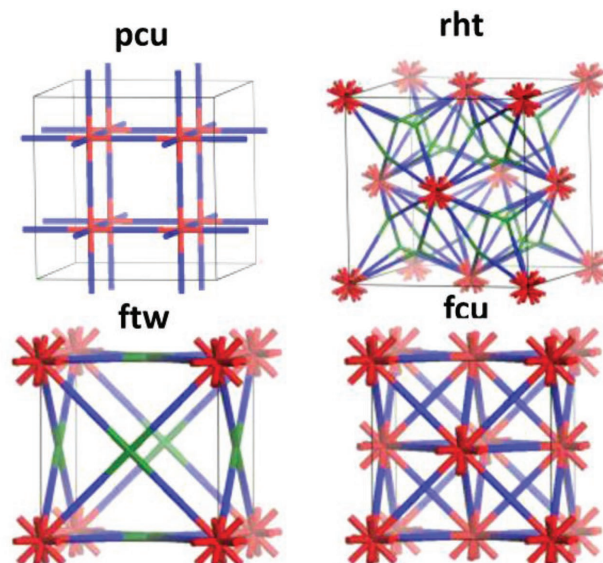


Figure 18. Representation of the topologies of MOFs discussed in this review. Reproduced with permission.^[123] Copyright 2016, American Chemical Society.

be considered. Based on the available literature in the state of the art, the main conclusion of this review are as follows:

- Bae et al.,^[110] Düren et al.,^[138] and Walton et al.^[56] found good agreement between the accessible surface areas and the BET surface areas calculated from N₂ or Ar adsorption isotherms for a series of MOFs with different sizes of pores where the consistency criteria were used. Contradictorily, Gómez-Gualdrón et al.^[123] claimed the agreement is not guaranteed by fulfilling the consistency criteria since deviations were observed (e.g., NU-110), despite achieving the criteria. Moreover, when the pressure range that did not

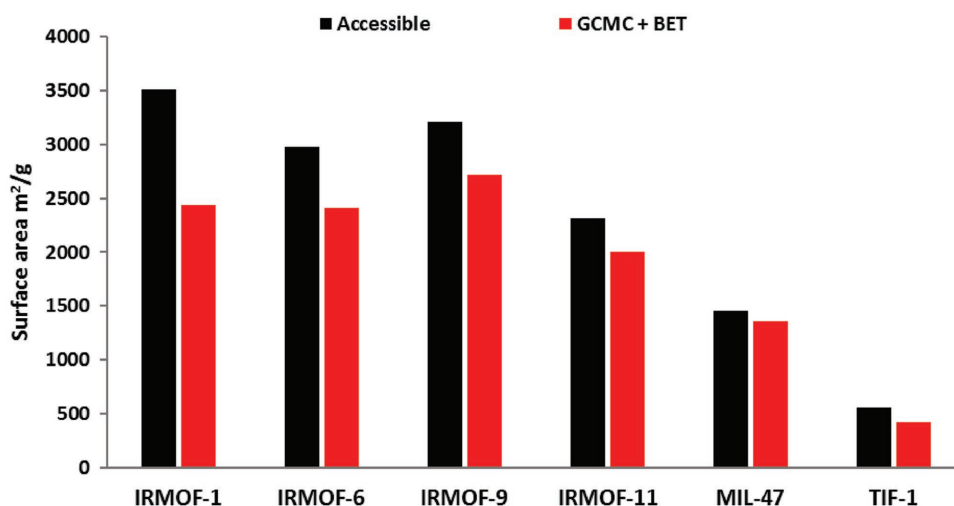


Figure 17. Comparison of the BET surface areas obtained from CO₂ adsorption isotherms versus geometrically calculated surface areas for six materials. The surface areas above the columns correspond to the absolute difference between the BET surface area and the surface area from the crystal structures. The deviation (%) was calculated by $[(\text{BET surface area} - \text{geometric surface area})/\text{geometric surface area}] \times 100$ ^[51] (Acronyms described in Table 3).

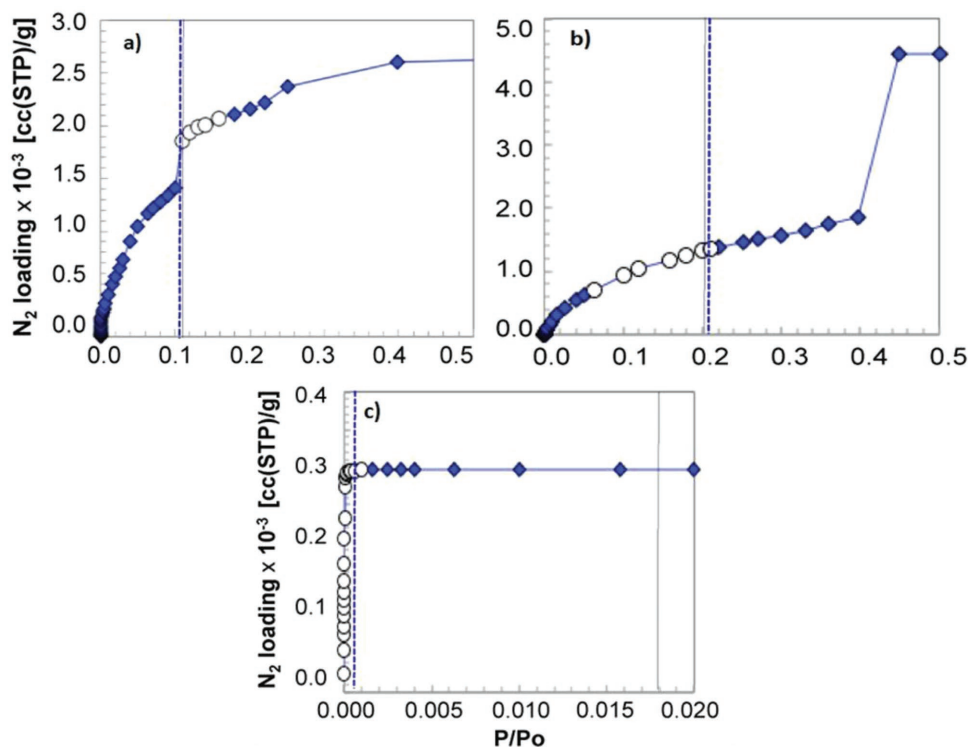


Figure 19. Simulated N_2 isotherms of a) NU-110, b) pcu-PPPP, and c) UiO-66. White symbols are related to points used for the BET surface area calculations; blue vertical lines represent the P/P_0 values related to the monolayer loading; black vertical lines represent the calculated values for the monolayer formation ($1/\sqrt{C} + 1$) and inset numbers indicate calculated pore diameters of materials. pcu-PPPP is a hypothetical MOF with pcu topology and four consecutive phenyl ring linkers. Reproduced with permission.^[123] Copyright 2016, American Chemical Society (Acronyms described in Table 3).

satisfy the 3rd and 4th aspect of the criteria chosen, the deviation did decrease for NU-110. In the same study it was also noted that the extent of agreement does not even depend on whether the criteria are fulfilled (e.g., UiO-67).^[123] Nevertheless, it is very important to use the criteria at least for consistency when comparing different materials.

- ii) Since the determination of the accessible surface area from the crystal structures of MOFs is a computationally inexpensive and a relatively quick method, Düren et al.^[138] stated

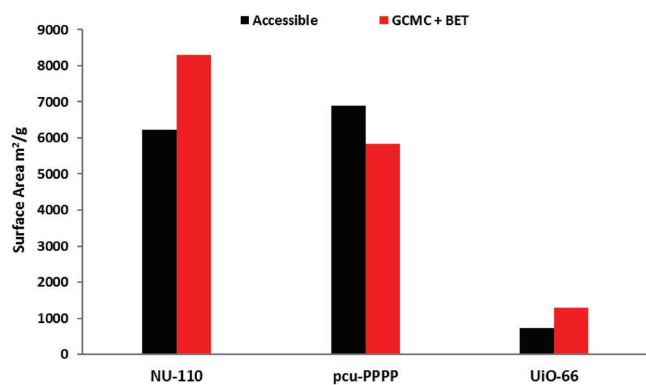


Figure 20. Simulated (GCMC) BET surface areas versus accessible surface areas for NU-110, pcu-PPPP, and UiO-66 (Acronyms described in Table 3).

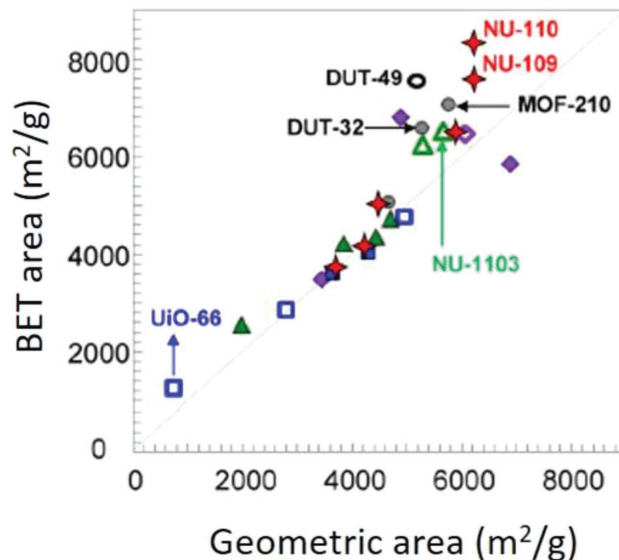


Figure 21. BET surface areas versus accessible surface areas of various types of MOFs that differ in topology; pcu (diamonds), fcu (squares), ftw (triangles), rht (stars), and other topologies (circles). Filled symbols represent the achieved consistency criteria while empty symbols relate to the unfulfilled consistency criteria. Reproduced with permission.^[123] Copyright 2016, American Chemical Society (Acronyms described in Table 3).

that they should be compared with the experimental surface areas since in their study, good comparisons were obtained. However, as stated by Gómez-Gualdrón et al.^[123] and Wang et al.,^[109] the experimental BET surface areas should be compared to simulated values obtained from GCMC simulations using the four consistency criteria and not against the accessible surface areas from the crystal structures.

- iii) For porous materials that exhibit polar heterogeneous surfaces, Ar molecule which has the absence of quadrupole moment is recommended over N₂ molecule for more reliable surface area determination and pore size analysis. Therefore, Ar adsorption at 87 K should be used, instead of N₂ adsorption at 77 K.
- iv) Since the correct determination of the true monolayer loading improves the agreement between the N₂ adsorption isotherm derived and the accessible surface area, the main challenge is to accurately estimate the molecular loading.^[123]
- v) For BET analysis, identification of the correct pressure range from adsorption isotherms is crucial, therefore they should be based on the four consistency criteria as suggested by Rouquerol et al.^[82] and not by simply using the “standard” BET pressure range ($0.05 < P/P_0 < 0.30$). Furthermore, since the BET surface area depends on the pressure range chosen, they should always be stated.
- vi) For certain MOFs (e.g., UiO-66, NU-110x series), it is not possible to satisfy every feature of the consistency criteria. However, in such instances every effort should be made to minimize the extent of deviation or use reasonable tolerances as suggested by Rouquerol et al.^[80] for the 4th aspect of the criteria (20% tolerance).
- vii) Defects in experimentally synthesized samples have often been associated with differences when comparing the experimentally determined BET and the accessible surface areas. However, this review has demonstrated that deviations can also come from incorrectly determining the pressure ranges on adsorption isotherms.
- viii) A computational study by Tian and Wu^[59] discovered that the BET surface areas are very sensitive to the characteristics of MOFs such as pore size, structure heterogeneity, and adsorbate–adsorbent interactions. Therefore, they indicated that the accessible surface areas are not correlated to the BET surface areas despite their good agreements in particular studies.
- ix) The deviations between the accessible surface areas based on CO₂ and the BET surface areas obtained from simulated CO₂ adsorption isotherms at 273 K for different types of MOFs were higher than for the same materials when N₂ or Ar gas was employed.

Based on the results discussed in this review, BET theory is a suitable approach for the determination of the surface area for microporous, crystalline materials that have their surface areas in the range of thousands m² g⁻¹ such as MOFs; however, specific limitations that were mentioned herein do exist.

Acknowledgements

The authors acknowledge financial support from Surface Measurement Systems Ltd. F.A., T.J.M., and I.P.P. would like to thank the Engineering and Physical Sciences Research Council (EPSRC) for financial support

(EP/L015862/1). T.J.M. would like to acknowledge the Ramsay Memorial Trust for their financial assistance. T.J.M. would also like to thank Dr. Munkhbayar Batmunkh for useful discussions regarding this review.

Conflict of Interest

The authors declare no conflict of interest.

Keywords

BET method, consistency criteria, MOFs, porous materials, surface area sizes

Received: May 31, 2018

Revised: July 1, 2018

Published online: August 16, 2018

- [1] H. B. Wu, X. W. (David) Lou, *Sci. Adv.* **2017**, *3*, eaap9252.
- [2] F. Moreau, I. da Silva, N. H. A. Smail, T. L. Easun, M. Savage, H. G. W. Godfrey, S. F. Parker, P. Manuel, S. Yang, M. Schröder, *Nat. Commun.* **2017**, *8*, 14085.
- [3] S. K. Elsaidi, M. H. Mohamed, D. Banerjee, P. K. Thallapally, *Coord. Chem. Rev.* **2018**, *358*, 125.
- [4] H.-C. Zhou, J. R. Long, O. M. Yaghi, *Chem. Rev.* **2012**, *112*, 673.
- [5] L. E. Kreno, K. Leong, O. K. Farha, M. Allendorf, R. P. Van Duyne, J. T. Hupp, *Chem. Rev.* **2012**, *112*, 1105.
- [6] S. L. James, *Chem. Soc. Rev.* **2003**, *32*, 276.
- [7] J. L. C. Rowsell, O. M. Yaghi, *Angew. Chem., Int. Ed.* **2005**, *44*, 4670.
- [8] M. Jurcic, W. J. Peveler, C. N. Savory, D. O. Scanlon, A. J. Kenyon, I. P. Parkin, *J. Mater. Chem. A* **2015**, *3*, 6351.
- [9] J. S. Seo, D. Whang, H. Lee, S. I. Jun, J. Oh, Y. J. Jeon, K. Kim, *Nature* **2000**, *404*, 982.
- [10] H. Zhao, Y. Chen, Q. Peng, Q. Wang, G. Zhao, *Appl. Catal., B* **2017**, *203*, 127.
- [11] S. Yuan, J.-S. Qin, J. Li, L. Huang, L. Feng, Y. Fang, C. Lollar, J. Pang, L. Zhang, D. Sun, A. Alsalme, T. Cagin, H.-C. Zhou, *Nat. Commun.* **2018**, *9*, 808.
- [12] M. Eddaoudi, J. Kim, N. Rosi, D. Vodak, J. Wachter, M. O’Keeffe, O. M. Yaghi, *Science* **2002**, *295*, 469.
- [13] M. Witman, S. Ling, A. Gladysiak, K. C. Stylianou, B. Smit, B. Slater, M. Haranczyk, *J. Phys. Chem. C* **2017**, *121*, 1171.
- [14] T. Tian, Z. Zeng, D. Vulpe, M. E. Casco, G. Divitini, P. A. Midgley, J. Silvestre-Albero, J.-C. Tan, P. Z. Moghadam, D. Fairen-Jimenez, *Nat. Mater.* **2018**, *17*, 174.
- [15] H. Furukawa, K. E. Cordova, M. O’Keeffe, O. M. Yaghi, *Science* **2013**, *341*, 1230444.
- [16] Y. Chen, D. Lv, J. Wu, J. Xiao, H. Xi, Q. Xia, Z. Li, *Chem. Eng. J.* **2017**, *308*, 1065.
- [17] F. Chen, Y. Wang, D. Bai, M. He, X. Gao, Y. He, *J. Mater. Chem. A* **2018**, *6*, 3471.
- [18] P. Horcajada, T. Chalati, C. Serre, B. Gillet, C. Sebrie, T. Baati, J. F. Eubank, D. Heurtaux, P. Clayette, C. Kreuz, J.-S. Chang, Y. K. Hwang, V. Marsaud, P.-N. Bories, L. Cynober, S. Gil, G. Ferey, P. Couvreur, R. Gref, *Nat. Mater.* **2010**, *9*, 172.
- [19] C. Orellana-Tavra, R. J. Marshall, E. F. Baxter, I. A. Lazaro, A. Tao, A. K. Cheetham, R. S. Forgan, D. Fairen-Jimenez, *J. Mater. Chem. B* **2016**, *4*, 7697.
- [20] X.-Y. Liu, F. Zhang, T.-W. Goh, Y. Li, Y.-C. Shao, L. Luo, W. Huang, Y.-T. Long, L.-Y. Chou, C.-K. Tsung, *Angew. Chem., Int. Ed.* **2018**, *57*, 2110.

- [21] M. D. Allendorf, C. A. Bauer, R. K. Bhakta, R. J. T. Houk, *Chem. Soc. Rev.* **2009**, 38, 1330.
- [22] S. Hu, L. Lv, S. Chen, M. You, Z. Fu, *Cryst. Growth Des.* **2016**, 16, 6705.
- [23] Y. Luo, S. Fan, W. Yu, Z. Wu, D. A. Cullen, C. Liang, J. Shi, C. Su, *Adv. Mater.* **2018**, 30, 1704576.
- [24] M. Alvaro, E. Carbonell, B. Ferrer, F. X. Llabrés i Xamena, H. Garcia, *Chem. – Eur. J.* **2007**, 13, 5106.
- [25] Y. Li, A. Pang, C. Wang, M. Wei, *J. Mater. Chem.* **2011**, 21, 17259.
- [26] Y. Li, L. Zhao, Z. Du, J. Du, W. Wang, Y. Wang, L. Zhao, X.-M. Cao, X. Zhong, *J. Mater. Chem. A* **2018**, 6, 2129.
- [27] F. Ambroz, T. J. Macdonald, T. Nann, *Adv. Energy Mater.* **2017**, 7, 1602093.
- [28] G. Zou, H. Hou, P. Ge, Z. Huang, G. Zhao, D. Yin, X. Ji, *Small* **2018**, 14, 1702648.
- [29] X. Zhou, J. Tian, J. Hu, C. Li, *Adv. Mater.* **2018**, 30, 1704166.
- [30] Q. Zhang, J. M. Shreeve, *Angew. Chem., Int. Ed.* **2014**, 53, 2540.
- [31] A. D. G. Firmino, F. Figueira, J. P. C. Tomé, F. A. A. Paz, J. Rocha, *Coord. Chem. Rev.* **2018**, 355, 133.
- [32] G. S. Papaefstathiou, L. R. MacGillivray, *Coord. Chem. Rev.* **2003**, 246, 169.
- [33] A. K. Das, R. S. Vemuri, I. Kutnyakov, B. P. McGrail, R. K. Motkuri, *Sci. Rep.* **2016**, 6, 28050.
- [34] D. P. Broom, M. Hirscher, *Energy Environ. Sci.* **2016**, 9, 3368.
- [35] H. Zhang, H. Osgood, X. Xie, Y. Shao, G. Wu, *Nano Energy* **2017**, 31, 331.
- [36] S. O. Odoh, C. J. Cramer, D. G. Truhlar, L. Gagliardi, *Chem. Rev.* **2015**, 115, 6051.
- [37] S. Amirjalayer, R. Schmid, *J. Phys. Chem. C* **2016**, 120, 27319.
- [38] J. Liang, Z. Liang, R. Zou, Y. Zhao, *Adv. Mater.* **2017**, 29, 1701139.
- [39] *Zeolites and Zeolite-like Materials* (Eds: B. F. Sels, L. M. Kustov), Elsevier, Amsterdam, **2016**, pp. i–ii.
- [40] B. M. Weckhuysen, J. Yu, *Chem. Soc. Rev.* **2015**, 44, 7022.
- [41] Z. Zhang, Z.-Z. Yao, S. Xiang, B. Chen, *Energy Environ. Sci.* **2014**, 7, 2868.
- [42] A. J. Howarth, A. W. Peters, N. A. Vermeulen, T. C. Wang, J. T. Hupp, O. K. Farha, *Chem. Mater.* **2017**, 29, 26.
- [43] T. Islamoglu, S. Goswami, Z. Li, A. J. Howarth, O. K. Farha, J. T. Hupp, *Acc. Chem. Res.* **2017**, 50, 805.
- [44] B. Y. Guan, X. Y. Yu, H. B. Wu, X. W. (David) Lou, *Adv. Mater.* **2017**, 29, 1703614.
- [45] P. Ghosh, *Colloid and Interface Science*, PHI Learning Pvt. Ltd., **2009**, <https://www.amazon.in/Colloid-Interface-Science-Ghosh/dp/812033857X>.
- [46] A. M. Grumezescu, *Design of Nanostructures for Theranostics Applications*, William Andrew, **2017**, https://books.google.si/books?id=XzAsDwAAQBAJ&dq=A.+M.+Grumezescu,+Design+of+Nanostructures+for+Theranostics+Applications,+William+Andrew,+2017&source=gbs_navlinks_s.
- [47] M. Gürsoy, M. Karaman, *Surface Treatments for Biological, Chemical and Physical Applications*, John Wiley & Sons, **2017**, https://books.google.si/books?id=rCl4DQAAQBAJ&dq=Surface+Treatments+for+Biological,+Chemical+and+Physical+Applications&source=gbs_navlinks_s.
- [48] G. Zhu, H. Ren, *Porous Organic Frameworks: Design, Synthesis and Their Advanced Applications*, Springer, **2014**, https://books.google.si/books?id=dZOeBQAAQBAJ&dq=Porous+Organic+Frameworks:+Design,+Synthesis+and+Their+Advanced+Applications&source=gbs_navlinks_s.
- [49] C. Racles, M.-F. Zaltariov, M. Iacob, M. Silion, M. Avadanei, A. Barga, *Appl. Catal., B* **2017**, 205, 78.
- [50] H. Kim, H. J. Cho, S. Narayanan, S. Yang, H. Furukawa, S. Schiffrès, X. Li, Y.-B. Zhang, J. Jiang, O. M. Yaghi, E. N. Wang, *Sci. Rep.* **2016**, 6, 19097.
- [51] K. C. Kim, T.-U. Yoon, Y.-S. Bae, *Microporous Mesoporous Mater.* **2016**, 224, 294.
- [52] M. F. de Lange, L.-C. Lin, J. Gascon, T. J. H. Vlucht, F. Kapteijn, *Langmuir* **2016**, 32, 12664.
- [53] B. Streppel, M. Hirscher, *Phys. Chem. Chem. Phys.* **2011**, 13, 3220.
- [54] H. Furukawa, N. Ko, Y. B. Go, N. Aratani, S. B. Choi, E. Choi, A. Ö. Yazaydin, R. Q. Snurr, M. O’Keeffe, J. Kim, O. M. Yaghi, *Science* **2010**, 329, 424.
- [55] I. Spanopoulos, I. Bratsos, C. Tampaxis, D. Vourloumis, E. Klontzas, G. E. Froudakis, G. Charalambopoulou, T. A. Steriotis, P. N. Trikalitis, *Chem. Commun.* **2016**, 52, 10559.
- [56] K. S. Walton, R. Q. Snurr, *J. Am. Chem. Soc.* **2007**, 129, 8552.
- [57] W. G. McMillan, E. Teller, *J. Phys. Chem.* **1951**, 55, 17.
- [58] D. Dollimore, P. Spooner, A. Turner, *Surf. Technol.* **1976**, 4, 121.
- [59] Y. Tian, J. Wu, *AIChE J.* **2018**, 64, 286.
- [60] P. S. Liu, G. F. Chen, *Porous Materials: Processing and Applications*, Butterworth-Heinemann, Boston **2014**, pp. 411–492.
- [61] P. C. Hiemenz, R. Rajagopalan, *Principles of Colloid and Surface Chemistry*, 3rd ed., CRC Press, **2016**, https://books.google.si/books?id=K6OKDQAAQBAJ&dq=Principles+of+Colloid+and+Surface+Chemistry,+Third+Edition,+Revised+and+Expanded&source=gbs_navlinks_s.
- [62] S. Lowell, J. E. Shields, M. A. Thomas, M. Thommes, *Characterization of Porous Solids and Powders: Surface Area, Pore Size and Density*, Springer Science & Business Media, **2012**, https://books.google.si/books?id=lwvSBwAAQBAJ&dq=Characterization+of+Porous+Solids+and+Powders:+Surface+Area,+Pore+Size+and+Density&source=gbs_navlinks_s.
- [63] J. Lyklema, *Fundamentals of Interface and Colloid Science: Solid-Liquid Interfaces*, Elsevier, **1995**, https://books.google.si/books?id=wH1A2zvIvQgC&dq=Fundamentals+of+Interface+and+Colloid+Science:+Solid-Liquid+Interfaces&source=gbs_navlinks_s.
- [64] R. G. Mortimer, *Physical Chemistry*, Academic Press, London, UK **2008**.
- [65] S. Brunauer, *The Adsorption of Gases and Vapors*, Physical Adsorption, Vol. I, Read Books, **2008**, https://books.google.si/books?id=jk9Q_5whmhYC&dq=The+Adsorption+of+Gases+and+Vapors+Vol+I++Physical+Adsorption&hl=en&sa=X&ved=0ahUKEwJ8xYjQ0eLcAhVMKuwKHRgcBagQ6AEIKDAA.
- [66] J.-K. Park, *Principles and Applications of Lithium Secondary Batteries*, John Wiley & Sons, **2012**, https://books.google.si/books?id=papHH-urMYC&dq=Principles+and+Applications+of+Lithium+Secondary+Batteries&source=gbs_navlinks_s.
- [67] A. T. Hubbard, *Encyclopedia of Surface and Colloid Science*, CRC Press, **2002**, https://books.google.si/books?id=GobXwAOZ1xcC&dq=Encyclopedia+of+Surface+and+Colloid+Science,&source=gbs_navlinks_s.
- [68] M. Che, *Characterization of Solid Materials and Heterogeneous Catalysts: From Structure to Surface Reactivity*, John Wiley & Sons, Weinheim, Germany **2012**.
- [69] B. Crittenden, W. J. Thomas, *Adsorption Technology and Design*, Elsevier, **1998**, https://books.google.si/books?id=ipDj12tyXfkC&dq=Adsorption+Technology+and+Design,&source=gbs_navlinks_s.
- [70] M. Cai, *Rock Mechanics: Achievements and Ambitions*, CRC Press, **2011**, https://books.google.si/books?id=nOSvdF6y21C&dq=Rock+Mechanics:+Achievements+and+Ambitions&source=gbs_navlinks_s.
- [71] S. Lowell, J. E. Shields, *Powder Surface Area and Porosity*, Springer Science & Business Media, New York, NY **2013**.
- [72] L.-S. Fan, C. Zhu, *Principles of Gas-Solid Flows*, Cambridge University Press, **2005**, https://books.google.si/books?id=zqUQBT2fMUYC&dq=Principles+of+Gas-Solid+Flows&source=gbs_navlinks_s.

- [73] W. A. Steele, G. Zgrablich, W. Rudzinski, *Equilibria and Dynamics of Gas Adsorption on Heterogeneous Solid Surfaces*, Elsevier, **1996**, https://books.google.si/books?id=BuPg3Oayi48C&dq=Equilibria+and+Dynamics+of+Gas+Adsorption+on+Heterogeneous+Solid+Surfaces&source=gbs_navlinks_s.
- [74] M. Thommes, K. Kaneko, A. V. Neimark, J. P. Olivier, F. Rodriguez-Reinoso, J. Rouquerol, K. S. W. Sing, *Pure Appl. Chem.* **2015**, *87*, 1051.
- [75] L. Chang-ha, *Adsorption Science And Technology: Proceedings of the Third Pacific Basin Conference*, World Scientific, **2003**, https://books.google.si/books?id=Ha3UCgAAQBAJ&dq=adsorption+Science+And+Technology:+Proceedings+of+the+Third+Pacific+Basin+Conference&source=gbs_navlinks_s.
- [76] J. M. Thomas, J. M. Thomas, W. J. Thomas, *Principles and Practice of Heterogeneous Catalysis*, John Wiley & Sons, **2015**, https://books.google.si/books?id=eFXWBgAAQBAJ&dq=Principles+and+Practice+of+Heterogeneous+Catalysis&source=gbs_navlinks_s.
- [77] J. García-Martínez, K. Li, *Mesoporous Zeolites: Preparation, Characterization and Applications*, John Wiley & Sons, **2015**, https://books.google.si/books?id=INxICQAAQBAJ&dq=Mesoporous+Zeolites:+Preparation,+Characterization+and+Applications,&source=gbs_navlinks_s.
- [78] U. Diwekar, *Batch Processing: Modeling and Design*, CRC Press, **2014**, https://books.google.si/books?id=uQ_lAgAAQBAJ&dq=Batch+Processing:+Modeling+and+Design&source=gbs_navlinks_s.
- [79] M. W. Hosseini, *Molecular Networks*, Springer Science & Business Media, **2009**, https://books.google.si/books?id=MP60FAYMUKc&dq=Molecular+Networks,+Springer+Science+%26+Business&source=gbs_navlinks_s.
- [80] J. Rouquerol, F. Rouquerol, P. Llewellyn, G. Maurin, K. S. W. Sing, *Adsorption by Powders and Porous Solids: Principles, Methodology and Applications*, Academic Press, **2013**, https://books.google.si/books?id=UOE-ZscYncC&dq=Adsorption+by+Powders+and+Porous+Solids:+Principles,+Methodology+and+Applications&source=gbs_navlinks_s.
- [81] M. D. LeVan, *Fundamentals of Adsorption: Proceedings of the Fifth International Conference on Fundamentals of Adsorption*, Springer Science & Business Media, **2012**, https://books.google.si/books?id=xlrSBwAAQBAJ&dq=Fundamentals+of+Adsorption:+Proceedings+of+the+Fifth+International+Conference+on+Fundamentals+of+Adsorption&source=gbs_navlinks_s.
- [82] J. Rouquerol, P. Llewellyn, F. Rouquerol, in *Studies in Surface Science and Catalysis* (Ed: F. Rodriguez-Reinoso, P. L. Llewellyn, J. Rouquerol, N. Seaton), Elsevier, **2007**, pp. 49–56, <https://www.sciencedirect.com/science/article/pii/S0167299107800085>.
- [83] C. R. A. Catlow, V. V. Speybroeck, R. van Santen, *Modelling and Simulation in the Science of Micro- and Meso-Porous Materials*, Elsevier, **2017**, https://books.google.si/books?id=afypDQAAQBAJ&dq=Modelling+and+Simulation+in+the+Science+of+Micro+and+Meso-Porous+Materials&source=gbs_navlinks_s.
- [84] B. C. Gates, F. C. Jentoft, *Advances in Catalysis*, Academic Press, **2013**, https://books.google.si/books?id=ld5lye37vtAC&dq=B.+C.+Gates,+F.+C.+Jentoft,+Advances+in+Catalysis&source=gbs_navlinks_s.
- [85] K. Sing, *Colloids Surf., A* **2001**, *187–188*, 3.
- [86] K. S. W. Sing, D. H. Everett, R. A. W. Haul, L. Moscou, K. A. Pierotti, J. Rouquerol, T. Simienicwska, *Pure Appl. Chem.* **1985**, *57*, 603.
- [87] L. D. Gelb, K. E. Gubbins, *Langmuir* **1998**, *14*, 2097.
- [88] A. Galarneau, H. Cambon, F. Di Renzo, F. Fajula, *Langmuir* **2001**, *17*, 8328.
- [89] J. L. C. Rowsell, O. M. Yaghi, *J. Am. Chem. Soc.* **2006**, *128*, 1304.
- [90] K. Kaneko, C. Ishii, *Colloids Surf.* **1992**, *67*, 203.
- [91] Y. Lou, P. He, L. Zhao, W. Cheng, H. Song, *Appl. Catal., B* **2017**, *201*, 278.
- [92] M. Linares, C. Vargas, A. García, C. Ochoa-Hernández, J. Čejka, R. A. García-Muñoz, D. P. Serrano, *Catal. Sci. Technol.* **2017**, *7*, 181.
- [93] M. H. Nada, S. C. Larsen, *Microporous Mesoporous Mater.* **2017**, *239*, 444.
- [94] M. Xu, Y. Wang, J. Geng, D. Jing, *Chem. Eng. J.* **2017**, *307*, 181.
- [95] B. Bajorowicz, J. Nadolna, W. Lisowski, T. Klimczuk, A. Zaleska-Medynska, *Appl. Catal., B* **2017**, *203*, 452.
- [96] J. Zhu, P.-Z. Li, W. Guo, Y. Zhao, R. Zou, *Coord. Chem. Rev.* **2018**, *359*, 80.
- [97] F. Leng, H. Liu, M. Ding, Q.-P. Lin, H.-L. Jiang, *ACS Catal.* **2018**, *8*, 4583.
- [98] X.-P. Wu, L. Gagliardi, D. G. Truhlar, *J. Am. Chem. Soc.* **2018**, *140*, 7904.
- [99] T. He, B. Ni, S. Zhang, Y. Gong, H. Wang, L. Gu, J. Zhuang, W. Hu, X. Wang, *Small* **2018**, *14*, 1703929.
- [100] J. G. Kim, T. J. Choi, J. Y. Chang, *Chem. Eng. J.* **2016**, *306*, 242.
- [101] S. Gu, J. He, Y. Zhu, Z. Wang, D. Chen, G. Yu, C. Pan, J. Guan, K. Tao, *ACS Appl. Mater. Interfaces* **2016**, *8*, 18383.
- [102] J. C. Bear, J. D. McGettrick, I. P. Parkin, C. W. Dunnill, T. Hasell, *Microporous Mesoporous Mater.* **2016**, *232*, 189.
- [103] M. Asemi, A. Suddar, M. Ghanaatshoar, *J. Mater. Sci. Mater. Electron.* **2017**, *28*, 15233.
- [104] S. Elmas, F. Ambroz, D. Chugh, T. Nann, *Langmuir* **2016**, *32*, 4952.
- [105] M. Batmunkh, T. J. Macdonald, C. J. Shearer, M. Bat-Erdene, Y. Wang, M. J. Biggs, I. P. Parkin, T. Nann, J. G. Shapter, *Adv. Sci.* **2017**, *4*, 1600504.
- [106] Y. Dou, J. Zhou, A. Zhou, J.-R. Li, Z. Nie, *J. Mater. Chem. A* **2017**, *5*, 19491.
- [107] R. P. Antony, A. K. Satpati, K. Bhattacharyya, B. N. Jagatap, *Adv. Mater. Interfaces* **2016**, *3*, 1600632.
- [108] T. J. Macdonald, F. Ambroz, M. Batmunkh, Y. Li, D. Kim, C. Contini, R. Poduval, H. Liu, J. G. Shapter, I. Papakonstantinou, I. P. Parkin, *Mater. Today Energy* **2018**, *9*, 254.
- [109] T. C. Wang, W. Bury, D. A. Gómez-Gualdrón, N. A. Vermeulen, J. E. Mondloch, P. Deria, K. Zhang, P. Z. Moghadam, A. A. Sarjeant, R. Q. Snurr, J. F. Stoddart, J. T. Hupp, O. K. Farha, *J. Am. Chem. Soc.* **2015**, *137*, 3585.
- [110] Y.-S. Bae, A. Ö. Yazaydin, R. Q. Snurr, *Langmuir* **2010**, *26*, 5475.
- [111] H. Khajavi, J. Gascon, J. M. Schins, L. D. A. Siebbeles, F. Kapteijn, *J. Phys. Chem. C* **2011**, *115*, 12487.
- [112] J. L. C. Rowsell, J. Eckert, O. M. Yaghi, *J. Am. Chem. Soc.* **2005**, *127*, 14904.
- [113] Z. Meng, R. Lu, D. Rao, E. Kan, C. Xiao, K. Deng, *Int. J. Hydrogen Energy* **2013**, *38*, 9811.
- [114] R. Richards, *Surface and Nanomolecular Catalysis*, CRC Press, **2006**, https://books.google.si/books?id=WunKBQAAQBAJ&dq=Surface+and+Nanomolecular+Catalysis&source=gbs_navlinks_s.
- [115] R. I. Masel, *Principles of Adsorption and Reaction on Solid Surfaces*, John Wiley & Sons, **1996**, https://books.google.si/books?id=c9bR3Mqg1lC&dq=of+Adsorption+and+Reaction+on+Solid+Surfaces,&source=gbs_navlinks_s.
- [116] L. Stewart, W. Lu, Z.-W. Wei, D. Ila, C. Padilla, H.-C. Zhou, *Dalton Trans.* **2017**, *46*, 14270.
- [117] W. Gao, T. Zhou, B. Louis, Q. Wang, *Catalysts* **2017**, *7*, 116.
- [118] S. J. Gregg, K. S. W. Sing, *Adsorption, Surface Area and Porosity*, Academic Press Inc, London **1982**.
- [119] *Fundam. Adsorpt.: Proc. Eng. Found. Conf.*, Schloss Elmau, Bavaria, West Germany, May 6–11, 1983, Engineering Foundation, New York, NY **1984**.
- [120] K. A. Cychosz, R. Guillet-Nicolas, J. García-Martínez, M. Thommes, *Chem. Soc. Rev.* **2017**, *46*, 389.
- [121] M. Thommes, K. A. Cychosz, *Adsorption* **2014**, *20*, 233.
- [122] H. Frost, T. Düren, R. Q. Snurr, *J. Phys. Chem. B* **2006**, *110*, 9565.

- [123] D. A. Gómez-Gualdrón, P. Z. Moghadam, J. T. Hupp, O. K. Farha, R. Q. Snurr, *J. Am. Chem. Soc.* **2016**, *138*, 215.
- [124] H. Shao, S. M. Lyth, *Hydrogen Energy Engineering*, Springer, Tokyo, **2016**, pp. 241–251.
- [125] H. K. Chae, D. Y. Siberio-Pérez, J. Kim, Y. Go, M. Eddaoudi, A. J. Matzger, M. O’Keeffe, O. M. Yaghi, *Nature* **2004**, *427*, 523.
- [126] R. L. Martin, M. Haranczyk, *Chem. Sci.* **2013**, *4*, 1781.
- [127] N. Huang, S. Yuan, H. Drake, X. Yang, J. Pang, J. Qin, J. Li, Y. Zhang, Q. Wang, D. Jiang, H.-C. Zhou, *J. Am. Chem. Soc.* **2017**, *139*, 18590.
- [128] S. Krause, V. Bon, U. Stoeck, I. Senkowska, D. M. Töbrens, D. Wallacher, S. Kaskel, *Angew. Chem., Int. Ed. Engl.* **2017**, *56*, 10676.
- [129] D. A. Gómez-Gualdrón, T. C. Wang, P. García-Holley, R. M. Sawelewa, E. Argueta, R. Q. Snurr, J. T. Hupp, T. Yildirim, O. K. Farha, *ACS Appl. Mater. Interfaces* **2017**, *9*, 33419.
- [130] https://books.google.si/books?id=qGuCb7RkV3gC&dq=A.+Blatov,+D.+M.+Proserpio,+in+Modern+Methods+of+Crystal+Structure+Prediction&source=gbs_navlinks_s.
- [131] J. Liu, L. Chen, H. Cui, J. Zhang, L. Zhang, C.-Y. Su, *Chem. Soc. Rev.* **2014**, *43*, 6011.
- [132] A. S. Münch, F. O. R. L. Mertens, *Microporous Mesoporous Mater.* **2018**, *270*, 180.
- [133] P. G. Yot, K. Yang, V. Guillermin, F. Ragon, V. Dmitriev, P. Parisiades, E. Elkaim, T. Devic, P. Horcajada, C. Serre, N. Stock, J. P. S. Mowat, P. A. Wright, G. Férey, G. Maurin, *Eur. J. Inorg. Chem.* **2016**, *2016*, 4424.
- [134] O. Karagiari, M. B. Lalonde, W. Bury, A. A. Sarjeant, O. K. Farha, J. T. Hupp, *J. Am. Chem. Soc.* **2012**, *134*, 18790.
- [135] K. Trepte, J. Schaber, S. Schwalbe, F. Drache, I. Senkowska, S. Kaskel, J. Kortus, E. Brunner, G. Seifert, *Phys. Chem. Chem. Phys.* **2017**, *19*, 10020.
- [136] V. Bon, I. Senkowska, I. A. Baburin, S. Kaskel, *Cryst. Growth Des.* **2013**, *13*, 1231.
- [137] O. K. Farha, I. Eryazici, N. C. Jeong, B. G. Hauser, C. E. Wilmer, A. A. Sarjeant, R. Q. Snurr, S. T. Nguyen, A. Ö. Yazaydin, J. T. Hupp, *J. Am. Chem. Soc.* **2012**, *134*, 15016.
- [138] T. Düren, F. Millange, G. Férey, K. S. Walton, R. Q. Snurr, *J. Phys. Chem. C* **2007**, *111*, 15350.
- [139] S. S.-Y. Chui, S. M.-F. Lo, J. P. H. Charmant, A. G. Orpen, I. D. Williams, *Science* **1999**, *283*, 1148.
- [140] F. Millange, C. Serre, G. Férey, *Chem. Commun.* **2002**, 822.
- [141] O. Weser, V. Veryazov, *Front. Chem.* **2017**, *5*, 111.
- [142] D. Lozano-Castelló, D. Cazorla-Amorós, A. Linares-Solano, *Carbon* **2004**, *42*, 1233.